Journal of
Composites Science

MDPI

Article

First Principle Study of Structural, Electronic, Optical Properties of Co-Doped ZnO

Ahmed Soussi [1,2,*], Redouane Haounati [3,*], Abderrahim Ait hssi [1], Mohamed Taoufiq [1], Abdellah Asbayou [1], Abdeslam Elfanaoui [1], Rachid Markazi [2], Khalid Bouabid [1] and Ahmed Ihlal [1]

[1] Materials and Renewable Energy Laboratory, Ibn Zohr University, Agadir 80000, Morocco
[2] High School of Technology-Guelmim, Ibn Zohr University, Agadir 80000, Morocco
[3] Laboratory of Organic and Physical Chemistry, Faculty of Science, Ibn Zohr University, Agadir 80000, Morocco
* Correspondence: ahmed.soussi@edu.uiz.ac.ma (A.S.); redouane.hay390@gmail.com (R.H.)

Abstract: In this theoretical study, the electronic, structural, and optical properties of copper-doped zinc oxide (CZO) were investigated using the full-potential linearized enhanced plane wave method (FP-LAPW) based on the density functional theory (DFT). The Tran–Blaha modified Becke–Johnson exchange potential approximation (TB-mBJ) was employed to enhance the accuracy of the electronic structure description. The introduction of copper atoms as donors in the ZnO resulted in a reduction in the material's band gap from 2.82 eV to 2.72 eV, indicating enhanced conductivity. This reduction was attributed to the Co-3d intra-band transitions, primarily in the spin-down configuration, leading to increased optical absorption in the visible range. The Fermi level of the pure ZnO shifted towards the conduction band, indicating metal-like characteristics in the CZO. Additionally, the CZO nanowires displayed a significant blue shift in their optical properties, suggesting a change in the energy band structure. These findings not only contribute to a deeper understanding of the CZO's fundamental properties but also open avenues for its potential applications in optoelectronic and photonic devices, where tailored electronic and optical characteristics are crucial. This study underscores the significance of computational techniques in predicting and understanding the behavior of doped semiconductors, offering valuable insights for the design and development of novel materials for advanced electronic applications.

Keywords: doped ZnO; FP-LAPW; bandgap; DOS; electronic properties; first principle study

Citation: Soussi, A.; Haounati, R.; Ait hssi, A.; Taoufiq, M.; Asbayou, A.; Elfanaoui, A.; Markazi, R.; Bouabid, K.; Ihlal, A. First Principle Study of Structural, Electronic, Optical Properties of Co-Doped ZnO. *J. Compos. Sci.* **2023**, *7*, 511. https://doi.org/10.3390/jcs7120511

Academic Editor: Zhong Hu

Received: 1 November 2023
Accepted: 4 December 2023
Published: 7 December 2023

1. Introduction

ZnO is a widely used material in many fields. It is a white crystalline powder with good transparency in the visible light range and is an indirect bandgap semiconductor [1,2]. ZnO is well known for its piezoelectric and photocatalytic properties and is used in a wide range of applications, including solar cells, transparent electrodes, sensors, and light-emitting diodes [3].

The CZO is a type of material that is of interest in a variety of applications such as sensing, energy harvesting, and water purification [4]. The presence of the Co dopants in the ZnO improves its electronic and optical properties, making it useful for these applications [5]. The doping process involves introducing a small amount of Co ions into the ZnO lattice to change its electrical conductivity and bandgap. This results in improved sensing and catalytic properties, making it an attractive material for various advanced technologies [6]. Moreover, the application of impurity-doped zinc oxide in transparent conductors (TCs) holds significant promise due to its impressive combination of electrical and optical properties, as cited in references [7–9]. The incorporation of donor elements, such as aluminum (Al), indium (In), gallium (Ga), tin (Sn), and silicon (Si), has been a widely explored method to enhance the electrical and optical characteristics of n-type ZnO

material, reaching concentrations of up to 10^{21} cm^{-3}. First principle studies have confirmed that specific dopants, like In, Al, and Ga, can improve the properties of ZnO films [10–12]. Recently, the enhancement of the ZnO bandgap energy through doping with elements such as Ca, Si, Ti, Co, Sc, and Mo has been reported [13–18]. Rare earth cations, including Tb, La, and Er dopants, demonstrate remarkable effectiveness in this regard [19,20]. This approach has paved the way for extensive research, with recent investigations focusing on the use of transition metals like vanadium (V) and niobium (Nb) as dopants for ZnO. These innovations have spurred a wave of exploration into the doped ZnO thin films, as indicated in references [21,22]. Furthermore, the ideal transparent conductive oxides (TCOs) must fulfill specific criteria to be effective. They should exhibit low absorption and reflectivity coefficients while maintaining a high transmittance across a broad spectrum, spanning from infrared (IR) to ultraviolet (UV) wavelengths. Additionally, these materials need to possess a high electrical conductivity. This comprehensive set of characteristics is crucial for various applications, including optoelectronics, solar cells, and displays, making ongoing research in this area particularly vital for advancing technology and scientific understanding.

The CZO has become an essential material in semiconductor research due to its fascinating electronic and magnetic properties [5,18]. The purposeful inclusion of cobalt ions within the ZnO lattice results in unique properties that have piqued considerable scientific interest. Integrating cobalt, a transition metal, into the ZnO semiconductor matrix not only modifies its electronic structure but also imparts magnetic characteristics, transforming the material from non-magnetic to ferromagnetic [23]. This transformation holds great promise for various technological applications, such as spintronics, magnetic sensors, and dilute magnetic semiconductors. Understanding the complex interaction between the cobalt dopants and the host ZnO lattice is essential to exploit the full potential of the CZO in these applications [18]. Against this background, this study examines in detail the electronic and magnetic properties of the CZO, shedding light on the fundamental mechanisms underlying its unique behavior and paving the way for innovative advances in semiconductor technology. Experimental and theoretical studies of the CZO are complementary approaches to understanding the properties and behavior of this material.

Experimental studies provide direct observations of the material's properties and behavior, while theoretical studies help to interpret and understand these observations, and to predict new properties that may be useful for various applications. Experimental studies on the CZO generally involve the synthesis of the material using various methods, such as the sol-gel process [2,24–26], hydrothermal [27,28], electrodeposition [22,29] and pulse laser deposition [30], and the characterization of its properties using techniques such as X-ray diffraction, transmission electron microscopy, and photoluminescence spectroscopy [31]. All these methods have their own advantages and disadvantages, and the choice of method depends on the specific application and desired properties of the CZO material. These studies provide valuable information on the structural and optical properties of the material and are often the starting point for theoretical studies.

Theoretical studies, using methods such as the density functional theory (DFT) and ab initio [32] calculations, provide valuable information on the electronic structure, optical properties, and defect behavior of the ZnO. By investigating fundamental interactions at atomic and electronic levels, theoretical studies not only improve our understanding of ZnO but also facilitate the design and development of new devices with enhanced efficiency and performance [1]. The density functional theory (DFT) calculations are a popular computational approach used to study the electronic and optical properties of materials, including thin films [32]. The DFT is a quantum mechanical method that calculates the electron density of a system based on the interactions between the electrons and nuclei of the material's atoms. By calculating the electron density, the DFT enables us to understand the optical properties of thin films, such as their refractive index and absorption coefficient [33]. A significant advantage of the DFT lies in its three-dimensional scalability, denoted as N^3 (where N represents the number of basic functions). In contrast, the ab initio methods

scale at N^4. Consequently, the DFT calculations are marginally faster and more accurate. More importantly, the DFT methods address a key drawback of the ab initio techniques like Hartree–Fock [34]: the complete neglect of electron correlation. Electron correlation, defined as the disparity between the Hartree–Fock energy and the exact solution of the Schrödinger equation, is partially accounted for by the DFT methods without requiring additional computational time [35]. Theoretical studies of the CZO generally involve the use of computational methods such as the density functional theory (DFT) and many-body perturbation theory (MBPT), on the other hand, provide a better understanding of the material's electronic and optical properties, and can be used to design and optimize the material for specific applications. For example, theoretical studies can be used to predict the band gap and electronic structure of the material, as well as the effect of different co-doping concentrations on these properties [36]. This information is not directly accessible through experimental studies and provides valuable insights into material behavior. The advantage of theoretical studies is that they provide a better understanding of material properties and behavior and can be used to design and optimize the material for specific applications.

The objective of this study is to examine the impact of co-doping on the structural, electronic, and optical properties of the ZnO. The analysis was carried out using the density functional theory (DFT) as implemented in WIEN2K (23.1) software [37]. The modified Becke–Johnson of Tran–Blaha (TB-mBJ) and Perdew–Burke–Ernzerhof Generalized Gradient Approximation (PBE-GGA) were utilized to perform the calculations [38,39]. The investigation focuses on the effects of co-doping concentration on the electronic structure, optical properties, and electrical properties of the ZnO.

2. Computational Methods

The current computation employs the full potential augmented plane wave (FP-LAPW) method [40] integrated into the WIEN2K software package [38]. This approach is rooted in the density functional theory (DFT) and is utilized for performing first-principle calculations.

The calculations were performed utilizing two approximations, namely the TB-mBJ and PBE-GGA. However, only the results obtained with the TB-mBJ approximations were presented, owing to their superior performance over the PBE-GGA functional. When compared to other theoretical methods and real-world data, these approximations enhance both the bandgap and optical properties. The TB-mBJ approximation was used to account for exchange–correlation effects, and the calculations were deemed convergent when the total system energy stabilized within a range of 10^{-5} Ry. A wavefunction cutoff magnitude of $R_{MT} \times K_{max} = 7.5$ was applied, with the cutoff energy set at -6.0 Ry. The valence wavefunctions inside the muffin-tin spheres were extended to $l_{max} = 10$, and the charge density was Fourier-extended to $G_{max} = 12$ (a.u.)$^{-1}$. For the undoped ZnO system, 450 k-points in the first Brillouin zone were used, following an $8 \times 8 \times 7$ Monkhorst–Pack (MP) grid, and a $4 \times 4 \times 2$ supercell was used. The anisotropic nature of the ordinary and extraordinary components in the ZnO compounds is a consequence of their tetragonal structure (where $a = b \neq c$) (see Figure 1), as demonstrated by the method [2]. To present our results accurately, we need to use three axes: the *x*-axis, the *y*-axis, and the *z*-axis. However, in our calculations, we found that a and b were equal, so the results for the *x*-axis and *y*-axis were identical. Consequently, we will present our results in the xx-plane, which is the plane that includes the *x*- and *y*-axes, as well as the *z*-axis in all our figures. Within the hexagonal unit cell depicted in Figure 1, there are two Zn atoms and two O atoms. The Zn atoms occupy the corners of a hexagon, whereas the O atoms are situated between the Zn atoms along the hexagonal axis.

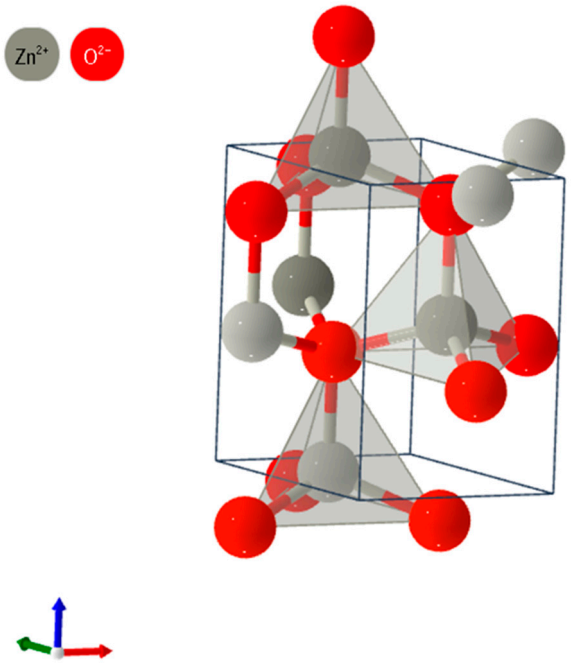

Figure 1. Zinc oxide (ZnO) unit cell in the F63mc space group.

3. Results and Discussion

3.1. Structural Properties

In the pursuit of determining the lattice equilibrium parameters, a meticulous process of structural optimization was undertaken for both the ZnO and CZO. This intricate task involved the application of the advanced WIEN2K software package, which facilitated the execution of self-consistent total energy calculations. To pinpoint the specific lattice parameters corresponding to the state of minimum energy, a systematic approach was adopted. This systematic approach included a series of steps, foremost among them being the rigorous minimization of the total energy. Through these comprehensive efforts, the precise lattice equilibrium parameters crucial for the study were successfully identified:

✓ Equilibrium volumes optimization: Optimizing equilibrium volumes involved a meticulous process of exploring the relationship between the total energy and unit cell volume for the studied ZnO compound. This exploration was conducted while keeping the atomic positions optimized and the experimental c/a ratio fixed. The cell volume was systematically varied within a range of ±15% of the reference volume (V_0). The resulting energy values for different volumes were analyzed and fitted using Murnaghan's equation (Equation (1)) to derive meaningful insights (See Figure 2).

$$E = \left[E_0 + \frac{BV}{B'} \left(\frac{\left(\frac{V}{V_0}\right)^{B'}}{B'+1} + 1 \right) - \frac{BV_0}{B'-1} \right] \quad (1)$$

where, B denotes the equilibrium bulk modulus, which characterizes the material's response to changes in pressure, and B′ represents its first derivative concerning ambient pressure. The term V_0 corresponds to the equilibrium unit cell volume, signifying the stable volume configuration attained under specific conditions.

✓ c/a ratio Optimization: Compute the total energy as a function of the c/a ratio through a systematic variation of ±5% in the c/a ratio, all while maintaining the theoretical equilibrium volume constant (See Figure 3).

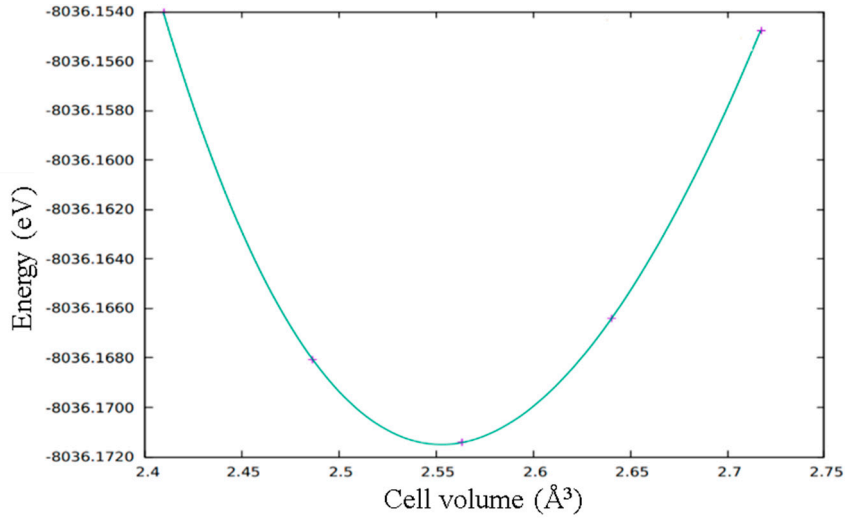

Figure 2. The total energy variation as a function of volume for the ZnO through a systematic variation of ±5%.

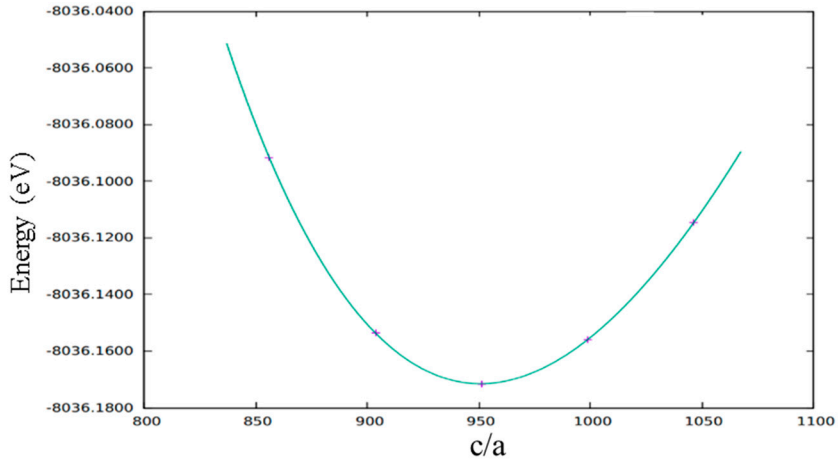

Figure 3. The total energy variation as a function of c/a for the ZnO through a systematic variation of ±15%.

The lattice parameters were determined based on the ground state, identified as the minimum of the total energy concerning the curves of cell volume and c/a ratio. The resulting values for lattice parameters a, c, and the c/a ratio, along with additional theoretical and experimental data, are provided in Table 1. Remarkably, our optimized lattice parameters align closely with both experimental values and results obtained from other theoretical approaches, indicating the accuracy and reliability of our findings.

Table 1. Various values of structural parameters of the pure ZnO and CZO.

		a = b (Å)	**c (Å)**	**c/a**
This work	ZnO	3.212	5.134	1.598
	CZO	3.220	5.190	1.611
experiments [1,5]	ZnO	3.247	5.196	1.600
	CZO	3.249	5.200	1.600
Other DFT works [2,36]	ZnO	3.230	5.160	1.597
	CZO	3.221	5.181	1.608

To examine the structural properties of the ZnO and CZO, the geometrical structures are shown in Figure 3 with space groups F63mc. It is noteworthy that the two geometrical structures have a tetragonal structure. The ZnO is wurtzite-structured and crystallizes in the hexagonal P63mc space group. The Zn^{2+} is bonded to four equivalent O^{2-} atoms to form corner-sharing ZnO_4 tetrahedra. There are three shorter (1.97 Å) and one longer (1.98 Å) Zn–O bond length. The O^{2-} is bonded to four equivalent Zn^{2+} atoms to form corner-sharing ZnO_4 tetrahedra (See Figure 1).

3.2. Electronic Properties

The electronic properties refer to the behavior and characteristics of materials in response to the flow of electric current, as well as the interaction of materials with electromagnetic fields. Understanding electronic properties is fundamental to various fields, including physics, materials science, electrical engineering, and chemistry. In the realm of electronic properties, two key concepts play a central role: conductivity and band structure.

Using supercell models, studies have been carried out on the CZO, where cobalt replaces zinc atoms at 2% cobalt concentration. The band structures of the pure ZnO and CZO are shown in Table 2. It can be seen that the band gap of the pure ZnO is 2.82 eV, in line with other reported measurements [2]. However, it is lower than the experimentally obtained value of 3.18 eV [2]. The theoretical bandgap value calculated for the Co-metal concentrations is 2.72 eV, which is lower than the value found for the host semiconductor.

Table 2. Various values of calculated and measured bandgap energy of ZnO and CZO.

		ZnO	**CZO**
This work	pbe-GGA	2.10	2.05
	TB-mBJ	2.82	2.72
Experiment [5]		3.20	3.02
Other DFT works	pbe-GGA [2,36]	2.34	1.12
	TB–mBJ [2]	2.64	
Band Gap nature		Direct	Direct

Our analysis determined that the bandgap values correspond to the states of the host semiconductor. We have observed in Figure 4 that the d-states are located within the band gap of the semiconductor. The empty cobalt states are now present in the conduction band and the filled states are located in the valence band.

As depicted in Figures 4 and 5, the incorporation of a cobalt ion into a ZnO semiconductor induces notable alterations in its properties. Specifically, this addition exerts a significant influence on both the material's band gap and the configuration of spin-up and spin-down states. Upon the introduction of a cobalt ion, the spin-up polarization interacts intricately with the valence band states, resulting in a considerable reduction in the band gap. This interaction also leads to the formation of distinct minority and majority levels linked to cobalt ions, especially noticeable under spin-down conditions.

This intriguing behavior is illustrated in the band structure shown in Figure 4 and the density of states (DOS) diagram provided in Figure 5. Together, these graphical representations effectively and efficiently capture the complex interplay between electronic states in the presence of cobalt ions, aligning perfectly with the results documented in the reference [23]. One of the key findings lies in the altered relationship between spin-up and spin-down states, highlighting the nuanced electronic behavior induced by the introduction of cobalt ions into the ZnO.

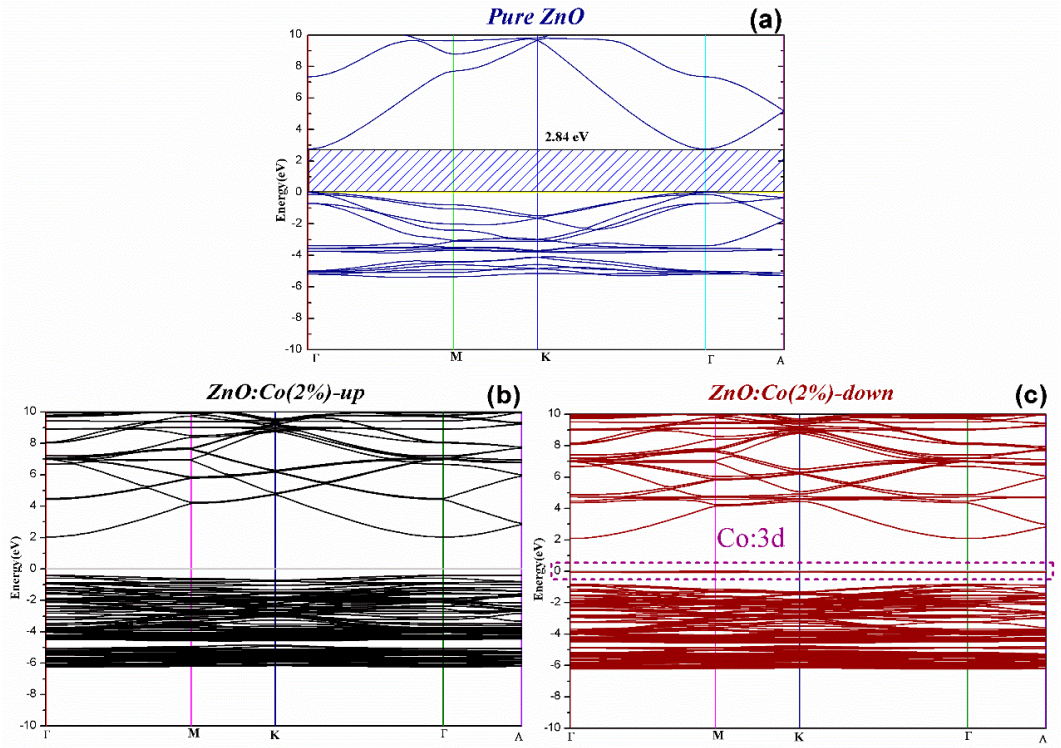

Figure 4. The band structures of ZnO (**a**) with 2% co-doping (**b**,**c**) along high-symmetry lines in the Brillouin zone using the TB-mBJ approximation.

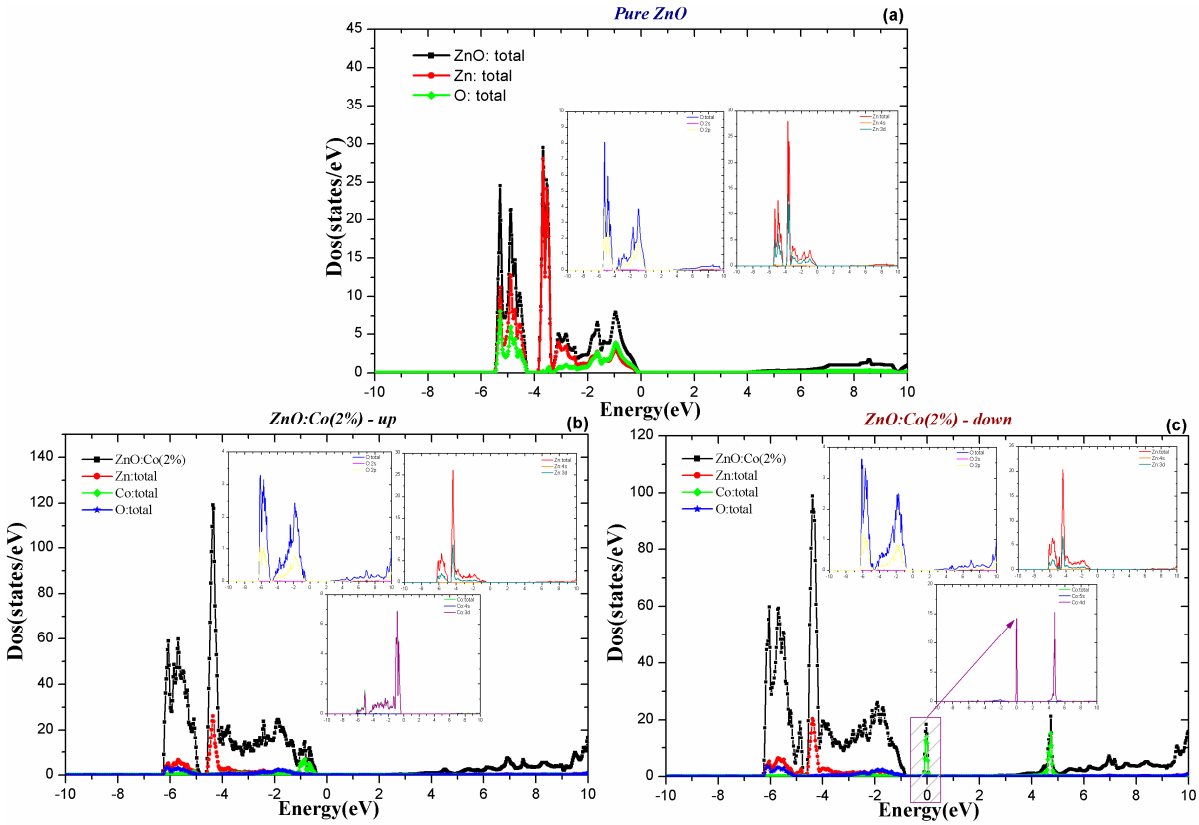

Figure 5. The densities of states of ZnO (**a**) with 2% co-doping (**b**,**c**) along high-symmetry lines in the Brillouin zone using the TB-mBJ approximation.

3.3. Optical Properties

Optical properties encompass the various interactions between material and light, including phenomena such as reflection, transmission, and absorption. The meticulous study of these properties in thin films is significant because of their versatility in a variety of applications, including optical coatings, solar cells, and electronic devices. These optical characteristics are closely related and can be exhaustively explained by the principles of wave optics. For example, the reflectivity, transmittance, and absorption of material collectively characterize the way light behaves as it passes through it. Studying the nuances of these optical properties not only improves our understanding but also enables us to precisely design and optimize materials for specific uses, from advanced optical coatings to solar cells and state-of-the-art electronic devices.

The dielectric function, defined by Equation (2), is a complex quantity that represents how a material reacts to an external electric field, and is closely related to the optical characteristics of the material [41,42]:

$$\varepsilon(\omega) = \varepsilon_1(\omega) + i\varepsilon_2(\omega) \tag{2}$$

The real and imaginary parts of the complex dielectric function are denoted as $\varepsilon_1(\omega)$ and $\varepsilon_2(\omega)$, respectively. The former is linked to the polarization and anomalous dispersion of the material, while the latter corresponds to the dissipation of energy in the medium. The real part of the dielectric function called the refractive index, determines the phase velocity of light in the material, while the imaginary part, called the extinction coefficient, determines the absorption of light by the material.

Using the dielectric function to calculate the optical properties of a material provides a convenient and flexible way of studying the behavior of light in materials, including light reflection, transmission, and absorption. The dielectric function can be obtained experimentally using spectroscopic techniques, such as ellipsometry or reflectometry, or theoretically using computational methods, such as density functional theory (DFT) or many-body perturbation theory. The real and imaginary parts of the dielectric function are related to the material's refractive index by Equation (2) [43–45]:

$$n(\omega) = \sqrt{\frac{\sqrt{\varepsilon_1(\omega)^2 + \varepsilon_2(\omega)^2} + \varepsilon_1(\omega)}{2}} \tag{3}$$

It is defined as the ratio between the speed of light in a vacuum and the speed of light in the material. A material with a high refractive index deflects more light than one with a low refractive index. According to Figure 6, the refractive index has a large value in the high-wavelength region (or low-energy region) but undergoes a considerable reduction in the low-wavelength region (or high-energy region).

The imaginary part of the dielectric function is related to the extinction coefficient by the Equation (4) [46]:

$$k(\omega) = \sqrt{\frac{\sqrt{\varepsilon_1(\omega)^2 + \varepsilon_2(\omega)^2} - \varepsilon_1(\omega)}{2}} \tag{4}$$

The extinction coefficient is a measure of the amount of light absorbed by a material as a function of the wavelength of the light. The extinction coefficient is proportional to the absorption coefficient and is often used to describe light absorption in a material in a more intuitive way. As shown in Figure 7, the extinction coefficient decreases with increasing wavelength, reaching low values in the visible and near-infrared range for both parallel and perpendicular components within the TB-mBJ approximations (See Figure 7).

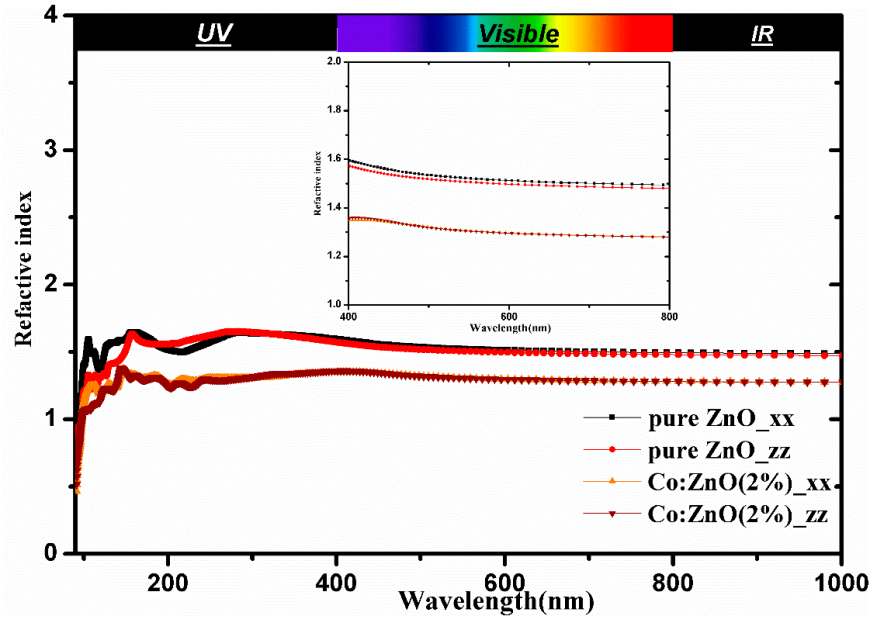

Figure 6. The refractive index calculated for the ZnO and CZO using the TB-mBJ approximation.

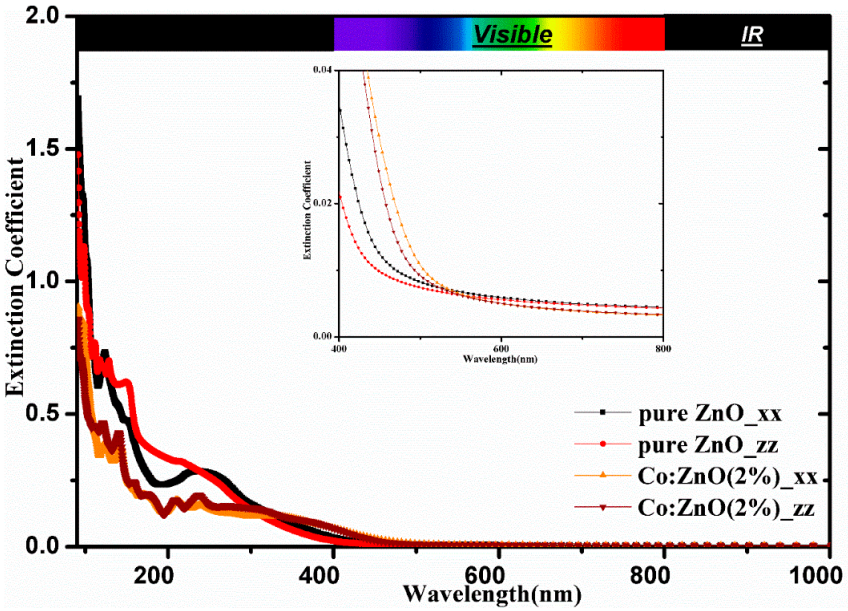

Figure 7. The extinction coefficient calculated for the ZnO and CZO using the TB-mBJ approximation.

Reflectivity and transmittance can be calculated using Fresnel's equations or the transfer matrix method, considering the refractive index and extinction coefficient of the material. The amount of light reflected by a surface is described by reflectivity, which is the ratio between the amount of light reflected and the amount of light incident on the surface. Figure 8 shows the reflectivity coefficient curves in the range from 0 to 13 eV. The calculation of reflectivity, R(ω), uses Equation (5) as shown in reference [43]:

$$R(\omega) = \left| \frac{\sqrt{\varepsilon_1(\omega) + j\varepsilon_2(\omega)} - 1}{\sqrt{\varepsilon_1(\omega) + j\varepsilon_2(\omega)} + 1} \right|^2 \quad (5)$$

Our findings reveal a distinct pattern in the behavior of the reflectivity coefficient. Specifically, we observed that the reflectivity coefficient attains its peak value in the UV range and gradually diminishes as the wavelength increases. This trend holds true for both

parallel and perpendicular components, as calculated within the TB-mBJ approximations. Furthermore, our analysis identified a noticeable anisotropy between the extraordinary and ordinary components of the reflectivity coefficient. This disparity underscores the directional dependence of the reflectivity properties, suggesting that the interaction of light with the material is not uniform in all directions. These observations provide valuable insights into the optical characteristics of the studied material and contribute to a deeper understanding of its behavior under different wavelengths and orientations.

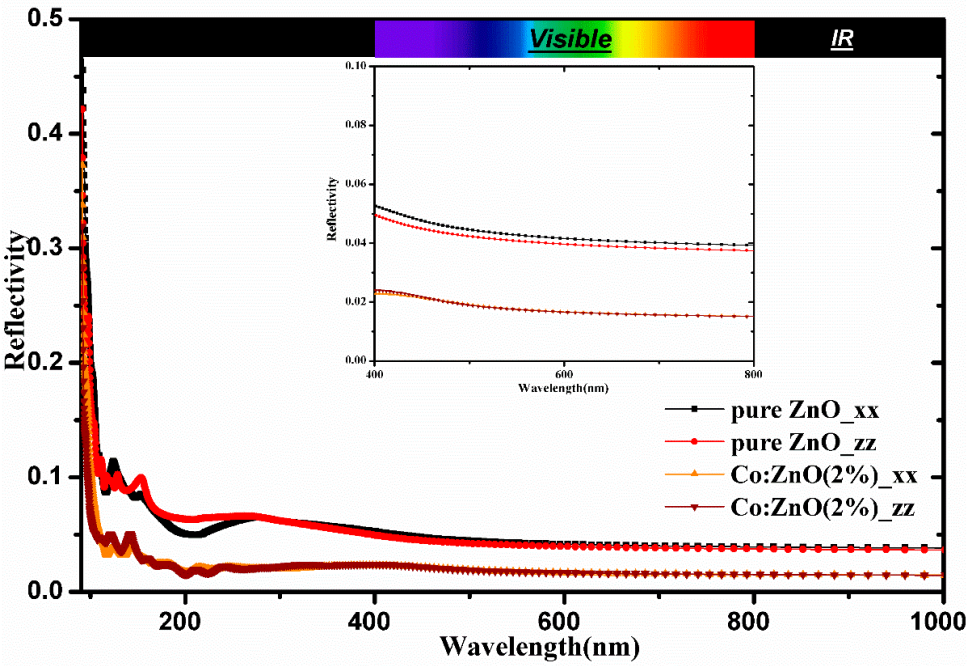

Figure 8. The reflectivity calculated for the ZnO and CZO using the TB-mBJ approximation.

The amount of light absorbed by a material is described by the absorption coefficient, which is a measure of the amount of light absorbed as a function of material thickness. Figure 9 illustrates the absorption coefficient, $\alpha(\omega)$, which is calculated directly from the dielectric function, and the correspondence used for this calculation is Equation (6) [47]:

$$\alpha(\omega) = \sqrt{2\left(\sqrt{\varepsilon_1(\omega)^2 + \varepsilon_2(\omega)^2} - \varepsilon_1(\omega)\right)} \quad (6)$$

In Figure 9, the peaks of the absorption spectrum correspond to the peaks of the imaginary part of the complex dielectric function, $\varepsilon_2(\omega)$. It is clear that for the photon energies below 3 eV, there is no absorption, as the curves start to decrease in the range above 400 nm for both the parallel and perpendicular components. The primary absorption peak is located in the UV range, between 0 and 200 nm.

Transmission refers to the phenomenon where light traverses through a substance. The measure of light that successfully passes through a material is defined by the transmission coefficient. This coefficient represents the ratio between the quantity of light that is transmitted through the material and the quantity of light that initially strikes the material's surface. The distinctive features observed in our study can be elucidated by the remarkably high transmission coefficients of the materials under investigation. Specifically, within the TB-mBJ approximation of the ZnO, the transmission coefficient surpasses 87% in both the visible and infrared regions. For the CZO, this coefficient rises to over 90%. These values are visually represented in Figure 10. Notably, at longer wavelengths beyond 380 nm, both materials exhibit exceptionally high transparency, signifying that they allow a significant portion of incident light to pass through without being absorbed or scattered.

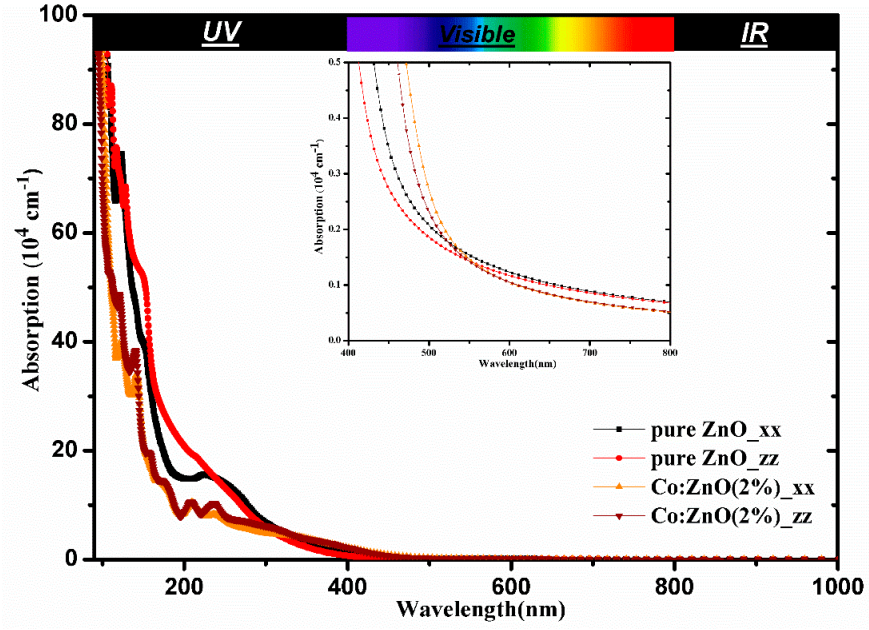

Figure 9. The absorption coefficient calculated for the ZnO and CZO using the TB-mBJ approximation.

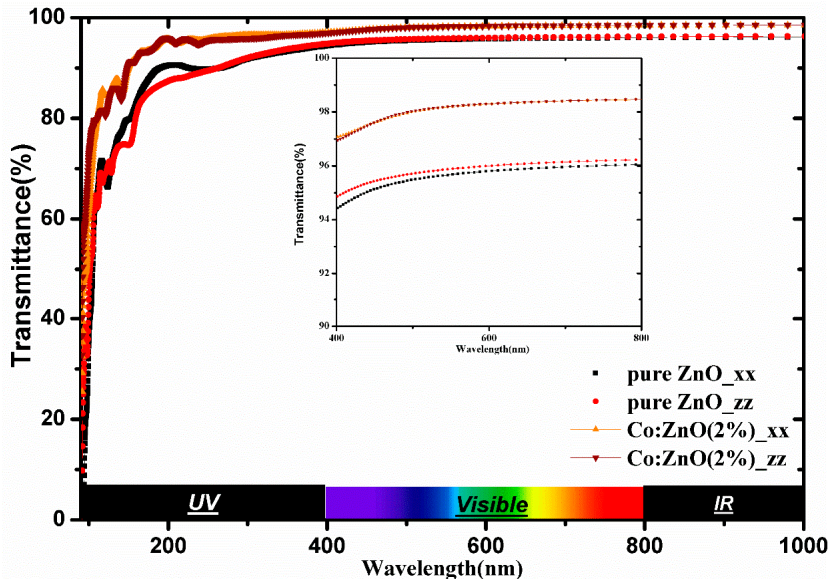

Figure 10. The transmittance calculated for the ZnO and CZO using the TB-mBJ approximation.

4. Conclusions

The effects of co-doping on the electronic and optical properties of the ZnO were explored with sophisticated first-principles calculations using density functional theory. This analysis was carried out both along the *z*-axis and in the xx-plane. To establish a basis for comparison, pure ZnO was used as the reference material. The tained using the TB-mBJ approach revealed that CZO exhibited characteristics typical of n-type metals. Using the same calculation method, the study demonstrated that co-doping significantly increased the absorption coefficient of the ZnO in the UV and visible spectra. This increase in visible light absorption was attributed to electron transfer from the O-2p state to the Co-3d state, as well as to intra-band transitions occurring between the Co-3d and Zn-3d states. The energy level associated with these intra-band transitions facilitated efficient electron transfer across interfaces and significantly reduced the rate of electron-hole recombination, particularly under sunlight, in the CZO. This phenomenon was corroborated by high transmission coefficients exceeding 90% in the visible range. As a result, the study concluded that the

co-doped rutile ZnO system exhibited enhanced photocatalytic activity. As a result, it emerged as a promising candidate for process applications. As a result, it has emerged as a promising candidate for applications in photoelectrochemical processes, representing a significant advance in this field.

Author Contributions: Conceptualization: A.S. and R.H.; Data curation: A.S., R.H. and A.A.h.; Formal analysis: A.S., A.E., A.A.h. and M.T.; Methodology: A.S., R.H., M.T. and A.A.; Validation: A.S., R.H., A.E. and R.M.; Visualization: A.S., A.E., R.M. and A.I.; Writing—original draft: A.S., A.A.h. and A.E.; Writing—review and editing: A.S., A.E., A.A.h., M.T., R.M., K.B. and A.I. All authors have read and agreed to the published version of the manuscript.

Funding: This research received no external funding.

Data Availability Statement: The datasets generated during and/or analyzed during the current study are available from the corresponding author.

Acknowledgments: The authors are grateful to P. Blaha and K. Schwarz at Wien Technical University for the Wien2k code and their kind reply.

Conflicts of Interest: The authors declare that they have no conflict of interest.

References

1. Soussi, A.; Labchir, N.; Taoufiq, M.; Najih, H.; Elfanaoui, A.; Ihlal, A.; Bouabid, K. A DFT Theoretical and Experimental Study of the Effect of Indium Doping within Electrochemical Deposited ZnO. *Vacuum* **2023**, *217*, 112503.
2. Soussi, A.; Boulkaddat, L.; Asbayou, A.; Labchir, N.; Elfanaoui, A.; Markazi, R.; Bouabid, K.; Ihlal, A.; Taleb, A. Structural, Optical and Electronic Properties of La-Doped ZnO Thin Films: Experimental Study and DFT Calculations. *Phys. B Condens. Matter.* **2022**, *643*, 414181. [CrossRef]
3. Haounati, R.; Ighnih, H.; Malekshah, R.E.; Alahiane, S.; Alakhras, F.; Alabbad, E.; Alghamdi, H.; Ouachtak, H.; Addi, A.A.; Jada, A. Exploring ZnO/Montmorillonite Photocatalysts for the Removal of Hazardous RhB Dye: A Combined Study Using Molecular Dynamics Simulations and Experiments. *Mater. Today Commun.* **2023**, *35*, 105915. [CrossRef]
4. Pelaez, M.; Nolan, N.T.; Pillai, S.C.; Seery, M.K.; Falaras, P.; Kontos, A.G.; Dunlop, P.S.M.; Hamilton, J.W.J.; Byrne, J.A.; O'Shea, K.; et al. A Review on the Visible Light Active Titanium Dioxide Photocatalysts for Environmental Applications. *Appl. Catal. B Environ.* **2012**, *125*, 331–349. [CrossRef]
5. Mahroug, A.; Boudjadar, S.; Hamrit, S.; Guerbous, L. Structural, Morphological and Optical Properties of Undoped and Co-Doped ZnO Thin Films Prepared by Sol–Gel Process. *J. Mater. Sci. Mater. Electron.* **2014**, *25*, 4967–4974. [CrossRef]
6. Yoshida, T.; Komatsu, D.; Shimokawa, N.; Minoura, H. Mechanism of Cathodic Electrodeposition of Zinc Oxide Thin Films from Aqueous Zinc Nitrate Baths. *Thin Solid Films* **2004**, *451*, 166–169. [CrossRef]
7. Scanlon, D.O.; Morgan, B.J.; Watson, G.W.; Walsh, A. Acceptor Levels in P-Type Cu_2O: Rationalizing Theory and Experiment. *Phys. Rev. Lett.* **2009**, *103*, 096405. [CrossRef]
8. Aragones, A.C.; Palacios-Padros, A.; Caballero-Briones, F.; Sanz, F. Study and Improvement of Aluminium Doped ZnO Thin Films: Limits and Advantages. *Electrochim. Acta* **2013**, *109*, 117–124. [CrossRef]
9. Pomoni, K.; Sofianou, M.V.; Georgakopoulos, T.; Boukos, N.; Trapalis, C. Electrical Conductivity Studies of Anatase TiO_2 with Dominant Highly Reactive {0 0 1} Facets. *J. Alloys Compd.* **2013**, *548*, 194–200. [CrossRef]
10. Hirata, G.A.; McKittrick, J.; Cheeks, T.; Siqueiros, J.M.; Diaz, J.A.; Contreras, O.; Lopez, O.A. Synthesis and Optelectronic Characterization of Gallium Doped Zinc Oxide Transparent Electrodes. *Thin Solid Films* **1996**, *288*, 29–31. [CrossRef]
11. Nunes, P.; Fernandes, B.; Fortunato, E.; Vilarinho, P.; Martins, R. Performances Presented by Zinc Oxide Thin Films Deposited by Spray Pyrolysis. *Thin Solid Films* **1999**, *337*, 176–179. [CrossRef]
12. Reddy, K.T.R.; Miles, R.W. Growth and Characterization of Sprayed ZnO: Ga Thin Films. *J. Mater. Sci. Lett.* **1998**, *17*, 279–281. [CrossRef]
13. Lin, S.-S.; Huang, J.-L.; Šajgalik, P. The Properties of Ti-Doped ZnO Films Deposited by Simultaneous RF and DC Magnetron Sputtering. *Surf. Coat. Technol.* **2005**, *191*, 286–292. [CrossRef]
14. Misra, K.P.; Shukla, R.K.; Srivastava, A.; Srivastava, A. Blueshift in Optical Band Gap in Nanocrystalline $Zn_{1-x}Ca_xO$ Films Deposited by Sol-Gel Method. *Appl. Phys. Lett.* **2009**, *95*, 31901. [CrossRef]
15. Minami, T.; Yamamoto, T.; Miyata, T. Highly Transparent and Conductive Rare Earth-Doped ZnO Thin Films Prepared by Magnetron Sputtering. *Thin Solid Films* **2000**, *366*, 63–68. [CrossRef]
16. Wu, C.; Shen, J.; Ma, J.; Wang, S.; Zhang, Z.; Yang, X. Electrical and Optical Properties of Molybdenum-Doped ZnO Transparent Conductive Thin Films Prepared by Dc Reactive Magnetron Sputtering. *Semicond. Sci. Technol.* **2009**, *24*, 125012. [CrossRef]
17. Lin, Y.-C.; Wang, B.L.; Yen, W.T.; Ha, C.T.; Peng, C. Effect of Process Conditions on the Optoelectronic Characteristics of ZnO: Mo Thin Films Prepared by Pulsed Direct Current Magnetron Sputtering. *Thin Solid Films* **2010**, *518*, 4928–4934. [CrossRef]

18. Subramanian, M.; Tanemura, M.; Hihara, T.; Ganesan, V.; Soga, T.; Jimbo, T. Magnetic Anisotropy in Nanocrystalline Co-Doped ZnO Thin Films. *Chem. Phys. Lett.* **2010**, *487*, 97–100. [CrossRef]
19. Kumari, V.; Kumar, V.; Malik, B.P.; Mehra, R.M.; Mohan, D. Nonlinear Optical Properties of Erbium Doped Zinc Oxide (EZO) Thin Films. *Opt. Commun.* **2012**, *285*, 2182–2188. [CrossRef]
20. Fang, Z.B.; Tan, Y.S.; Gong, H.X.; Zhen, C.M.; He, Z.W.; Wang, Y.Y. Transparent Conductive Tb-Doped ZnO Films Prepared by Rf Reactive Magnetron Sputtering. *Mater. Lett.* **2005**, *59*, 2611–2614. [CrossRef]
21. Boujnah, M.; Boumdyan, M.; Naji, S.; Benyoussef, A.; El Kenz, A.; Loulidi, M. High Efficiency of Transmittance and Electrical Conductivity of V Doped ZnO Used in Solar Cells Applications. *J. Alloys Compd.* **2016**, *671*, 560–565. [CrossRef]
22. Abouabassi, K.; Sala, A.; Atourki, L.; Soussi, A.; Elfanaoui, A.; Kirou, H.; Hssi, A.A.; Bouabid, K.; Gilioli, E.; Ihlal, A. Electrodeposited $CuSbSe_2$ Thin Films Based Solar Cells on Various Substrates. *J. Nanopart. Res.* **2022**, *24*, 1–10. [CrossRef]
23. Yang, S.; Zhang, Y. Structural, Optical and Magnetic Properties of Mn-Doped ZnO Thin Films Prepared by Sol-Gel Method. *J. Magn. Magn. Mater.* **2013**, *334*, 52–58. [CrossRef]
24. Hamrit, S.; Djessas, K.; Brihi, N.; Briot, O.; Moret, M.; Ben Ayadi, Z. Study and Optimization of Al-Doped ZnO Thin Films Deposited on PEN Substrates by RF-Magnetron Sputtering from Nanopowders Targets. *J. Mater. Sci. Mater. Electron.* **2016**, *27*, 1730–1737. [CrossRef]
25. Agarwal, L.; Sambasiva Rao, K.; Srivastava, A.; Tripathi, S. Ytterbium Doped ZnO Nanolaminated Planar Waveguide for Ring Resonator Applications. *J. Phys. D Appl. Phys.* **2022**, *55*, 225106. [CrossRef]
26. Soussi, A.; Elfanaoui, A.; Taoufiq, M.; Asbayou, A.; Boulkaddat, L.; Labchir, N.; Markazi, R.; Ihlal, A.; Bouabid, K. Morphological, Structural, Electronic and Optical Properties of Deposited 4d-Mo Doped TiO_2 Thin Films Compared to First-Principles Calculations. *Mater. Today Commun.* **2023**, *36*, 106520. [CrossRef]
27. Zhang, Y.H.; Cai, X.L.; Li, Y.L.; Liu, M.M.; Ding, C.L.; Chen, J.L.; Fang, S.M. Facile Synthesis of Hollow P-Cu_2O/n-ZnO Microspheres with Enhanced Photocatalytic H_2 Production. *Chem. Phys. Lett.* **2019**, *734*, 136748. [CrossRef]
28. Tlemcani, T.S.; Justeau, C.; Nadaud, K.; Poulin-Vittrant, G.; Alquier, D. Deposition Time and Annealing Effects of ZnO Seed Layer on Enhancing Vertical Alignment of Piezoelectric ZnO Nanowires. *Chemosensors* **2019**, *7*, 7. [CrossRef]
29. Amaterz, E.; Soussi, A.; Elfanaoui, A.; Benlhachemi, A.; Ihlal, A.; Bouabid, K. Electrodeposition of Nanostructured Cuprous Oxide on Various Substrates and Their Electrochemical and Photoelectrochemical Properties. *J. Mater. Sci. Mater. Electron.* **2022**, *33*, 15791–15801.
30. Beckford, J.; Behera, M.K.; Yarbrough, K.; Obasogie, B.; Pradhan, S.K.; Bahoura, M. Gallium Doped Zinc Oxide Thin Films as Transparent Conducting Oxide for Thin-Film Heaters. *AIP Adv.* **2021**, *11*, 075208. [CrossRef]
31. Bakhtiargonbadi, F.; Esfahani, H.; Moakhar, R.S.; Dabir, F. Fabrication of Novel Electrospun Al and Cu Doped ZnO Thin Films and Evaluation of Photoelectrical and Sunlight-Driven Photoelectrochemical Properties. *Mater. Chem. Phys.* **2020**, *252*, 123270. [CrossRef]
32. Bartlett, R.J. Adventures in DFT by a Wavefunction Theorist. *J. Chem. Phys.* **2019**, *151*, 160901. [CrossRef]
33. Hamideddine, I.; Zitouni, H.; Tahiri, N.; El Bounagui, O.; Ez-Zahraouy, H. A DFT Study of the Electronic Structure, Optical, and Thermoelectric Properties of Halide Perovskite $KGeI_{3-x}Br_x$ Materials: Photovoltaic Applications. *Appl. Phys. A* **2021**, *127*, 443. [CrossRef]
34. Fahmi, A.; Minot, C.; Silvi, B.; Causá, M. Theoretical Analysis of the Structures of Titanium Dioxide Crystals. *Phys. Rev. B* **1993**, *47*, 11717–11724. [CrossRef] [PubMed]
35. Guan, M.; Chen, D.; Hu, S.; Zhao, H.; You, P.; Meng, S. Theoretical Insights into Ultrafast Dynamics in Quantum Materials. *Ultrafast Sci.* **2022**, *2022*, 9767251. [CrossRef]
36. Zhang, F.; Cui, H.; Zhang, W. Identifying Properties of Co-Doped ZnO Nanowires from First-Principles Calculations. *Vacuum* **2015**, *119*, 131–135. [CrossRef]
37. Blaha, P.; Schwarz, K.; Madsen, G.K.H. *WIEN2K, An Augmented Plane Wave+ Local Orbitals Program for Calculating Crystal Properties*; TU Wien: Vienna, Austria, 2001; ISBN 3-9501031-1-2.
38. Schwarz, K.; Blaha, P. Solid State Calculations Using WIEN2k. *Comput. Mater. Sci.* **2003**, *28*, 259–273. [CrossRef]
39. Koller, D.; Tran, F.; Blaha, P. Merits and Limits of the Modified Becke-Johnson Exchange Potential. *Phys. Rev. B-Condens. Matter Mater. Phys.* **2011**, *83*, 195134. [CrossRef]
40. Blaha, P.; Schwarz, K.; Sorantin, P.; Trickey, S.B. Full-Potential, Linearized Augmented Plane Wave Programs for Crystalline Systems. *Comput. Phys. Commun.* **1990**, *59*, 399–415. [CrossRef]
41. Lee, C.; Gonze, X. Dielectric Constants and Born Effective Charges of TiO_2 Rutile. *Phys. Rev. B* **1994**, *49*, 14730–14731. [CrossRef]
42. Iqbal Khan, M.J.; Kanwal, Z. Investigation of Optical Properties of CdS for Various Na Concentrations for Nonlinear Optical Applications (A DFT Study). *Optik* **2019**, *193*, 162985. [CrossRef]
43. Sun, J.; Wang, H.T.; He, J.; Tian, Y. Ab Initio Investigations of Optical Properties of the High-Pressure Phases of ZnO. *Phys. Rev. B-Condens. Matter Mater. Phys.* **2005**, *71*, 125132. [CrossRef]
44. Yakuphanoglu, F.; Cukurovali, A.; Yilmaz, I. Refractive Index and Optical Absorption Properties of the Complexes of a Cyclobutane Containing Thiazolyl Hydrazone Ligand. *Opt. Mater.* **2005**, *27*, 1363–1368. [CrossRef]
45. Hadjab, M.; Berrah, S.; Abid, H.; Ziane, M.I.; Bennacer, H.; Reshak, A.H. First-Principles Investigation of the Optical Properties for Rocksalt Mixed Metal Oxide $Mg_xZn_{1-x}O$. *Mater. Chem. Phys.* **2016**, *182*, 182–189. [CrossRef]

46. Adewale, A.A.; Chik, A.; Adam, T.; Joshua, T.M.; Durowoju, M.O. Optoelectronic Behavior of ZnS Compound and Its Alloy: A First Principle Approach. *Mater. Today Commun.* **2021**, *27*, 102077. [CrossRef]
47. Ozaki, S.; Adachi, S. Optical Constants of ZnS_xSe_{1-x} Ternary Alloys. *J. Appl. Phys.* **1994**, *75*, 7470–7475. [CrossRef]